Journal of Molecular Structure 1292 (2023) 136193

Contents lists available at ScienceDirect

Journal of Molecular Structure

journal homepage: www.elsevier.com/locate/molstr

Supramolecular characterisation of salts of 4-(2-methoxyphenyl) piperazin-1-ium and 4-phenylpiperazin-1-ium cations with simple-organic anions; a closer look at the binding energies of cation-anion pairs formed by charge-assisted (+)N−H···O(-) and (+)N−H···O hydrogen bonds

Holehundi J. Shankara Prasad [a], Haleyur G. Anil Kumar [b], Thaluru M. Mohan Kumar [c], Channappa N. Kavitha [d], Devaraju [a], Hemmige S. Yathirajan [e,*], Sean R. Parkin [f], Lilianna Chęcińska [g,*]

[a] Department of Chemistry, Yuvaraja's College, University of Mysore, Mysore 570 005, India
[b] Department of Science and Humanities, PES University, BSK III Stage, Bengaluru 560 085, India
[c] Department of Chemistry, Amrita School of Engineering, Amrita Vishwa Vidyapeetham, Bengaluru 560 035, India
[d] Department of Chemistry, Government Science College, Hassan 573 201, India
[e] Department of Studies in Chemistry, University of Mysore, Manasagangotri, Mysore 570 006, India
[f] Department of Chemistry, University of Kentucky, Lexington, KY 40506, USA
[g] Faculty of Chemistry, University of Lodz, Lodz 90-236, Poland

ARTICLE INFO

Keywords:
Arylpiperazines
Supramolecular assembly
Binding energy
Charge-assisted hydrogen bond

ABSTRACT

Six new salts prepared by acid-base reactions containing 4-(2-methoxyphenyl)piperazin-1-ium cation (2-MeOPP) with simple organic-acid anions, namely pentafluorobenzoate, (I); (2*R*,3*R*)-tartrate dihydrate, (II); succinate trihydrate, (III); or 4-phenylpiperazin-1-ium cation (PP) with 4-chlorobenzoate monohydrate, (IV); 3-chlorobenzoate monohydrate, (V) and succinate (VI) have been structurally characterised using single-crystal X-ray diffraction. Crystal-packing architectures have been described in the context of the supramolecular assemblies they form. The most important structural motifs are generated through hydrogen bonds between 2-MeOPP or PP cations and associated anions, assisted by their charges. To quantify these charge-assisted hydrogen bonds: (+)N−H····O(-) and (+)N−H····O, the binding energies of the ionic pairs have been calculated and compared. We considered a set of 72 ionic pairs of the structures analysed in this article and those published previously by our groups. As a result, we have plotted lines of trends found for DFT-binding energies vs normalised H···O proton···acceptor distances, and correlation between normalised geometrical parameters for aromatic and aliphatic anions. A comparison between DFT-energies and model pairwise energies (CE-B3LYP) has also been made.

1. Introduction

Piperazines and their derivatives are important heterocycles in drug design studies that have been identified in biologically active compounds in a number of different therapeutic areas [1–3]. They draw a lot of attention because of their structural versatility [4,5]. Among the wide group of piperazine compounds, the phenylpiperazine (PP) framework has been found to have applications as anticancer agents for prostate cancer [6] or as active ingredients against many subtypes of serotonin receptors [7,8]. Similarly, *N*-(2-methoxyphenyl)piperazine (2-MeOPP) plays a significant role as a building block in the syntheses of dopamine D2 and D3 ligands [9] and compounds exhibiting antidepressant-like activity [10].

Our study is a continuation of our research work focused on the design, synthesis and determination of the crystal architecture of salts prepared by acid-base reactions using an equimolar mixture of *N*-(2-methoxyphenyl)piperazine (2-MeOPP) or 1-phenylpiperazine (PP) with organic acids. In this article, we present the structural characterization of three salts each of the aforementioned 2-MeOPP and PP cations with simple organic-acid anions, namely pentafluorobenzoate, (I); tartrate, (II); succinate, (III) and (VI); 4-chlorobenzoate, (IV); and 3-chlorobenzoate, (V) (Scheme 1). Recently, we have reported the crystal

* Corresponding authors.
E-mail addresses: yathirajan@hotmail.com (H.S. Yathirajan), lilianna.checinska@chemia.uni.lodz.pl (L. Chęcińska).

https://doi.org/10.1016/j.molstruc.2023.136193
Received 21 May 2023; Received in revised form 4 July 2023; Accepted 11 July 2023
Available online 12 July 2023
0022-2860/© 2023 Elsevier B.V. All rights reserved.

structures of fifteen salts of each cation, 2-MeOPP [11] and PP [12,13], respectively. Such a large amount of real structural data provided a unique opportunity to systematically analyse the driving force leading to these crystalline materials, which is known as a charge-assisted hydrogen bond (CAHB).

Different types of CAHB can be classified on the basis of the formal charge distribution in hydrogen bonding [14]. Thus, the CAHBs(+) are formed between proton-donating cations, which interact with the formally neutral proton-accepting group, while the CAHBs(-) show the opposite situation, in which the only acceptor is formally negatively charged. A combination of both types gives double charge-assisted hydrogen bonds (CAHB(+/-), sometimes called salt bridges, since they are characteristic for proton-transfer ionic pairs in salts. During the last few decades, many compounds with crystal architectures controlled by CAHBs have been reported, for example [15–17]; or the nature of interactions has been theoretically examined [18–20]. Collectively, these reports illustrate that charge-assisted hydrogen bonds of all types are effective for crystal design, and the exceptional strength of these interactions can produce supramolecular networks that can withstand the strains of other competing packing forces in the crystal structure [21, 22].

The significance of networks constructed with CAHB is well illustrated by the comprehensive series of salts based on the 2-MeOPP and PP cations and numerous anions synthesised in our laboratory. The positively charged N atom of the piperazine moiety forms two types of CAHBs with anions: (+)N−H····O(-) and (+)N−H····O, which are responsible for the formation of basic motifs and consequently for supramolecular assemblies of the structures analysed. To explore such interactions for each selected cation-anion pair (the cation-water/anion-water pairs have been omitted), we estimated the counterpoise-corrected binding energies identified with intermolecular hydrogen-bond energies. As a result, we have plotted relationships of the obtained energies vs normalised geometric parameters of all bridges. Furthermore, for ionic pairs of compounds (II), (IV) – (VI) the model energies have been calculated using the *CrystalExplorer* approach (CE-B3LYP energies) [23,24] and a comparison of CE-B3LYP vs DFT-energies has been made.

2. Materials and methods

2.2. Synthesis

All reagents were obtained commercially and were used as received. For the synthesis of the salts, equimolar quantities (0.52 mmol of each component) of *N*-(2-methoxyphenyl)piperazine (100 mg) (from Sigma-Aldrich) and pentafluorobenzoic acid (110 mg) / tartaric acid (78 mg) / succinic acid (61 mg) were separately dissolved in methanol (10 ml) and also equimolar quantities (0.62 mmol of each component) of 1-phenylpiperazine (100 mg) (from Sigma-Aldrich) and 4-chlorobenzoic acid (97 mg) / 3-chlorobenzoic acid (97 mg) / succinic acid (73 mg) were separately dissolved in methanol (10 ml) and the two solutions were then mixed, and stirred briefly at 333 K and then set aside to crystallize, giving the solid products (I) to (VI) after a few days. The products were collected by filtration and then dried in air (I: yield: 85%; m.p.: 396–398 K; II: yield: 75%; m.p.: 386–388 K; III: yield: 80%; m.p.: 377–379 K; IV: yield: 70%; m.p.: 397–399 K; V: yield: 75%; m.p.: 365–367 K; VI: yield: 75%; m.p.: 427–429 K;). Crystals of compounds (I to VI) suitable for single-crystal X-ray diffraction were grown by slow evaporation, at ambient temperature and in the presence of air, of solutions in methanol–acetonitrile (initial composition 1:1, v/v) for (I) – (III) and methanol-ethylacetate (initial composition 1:1, v/v) for (IV) – (VI).

2.3. X-ray single-crystal data collection

The crystal structures of (I) – (VI) were determined by single-crystal X-ray diffraction. Experiments were carried out at 90 K with Mo*K*α (I, III, IV, V) or Cu*K*α radiation (II, VI) using a Bruker D8 Venture diffractometer. Data collections, cell refinements and data reductions were

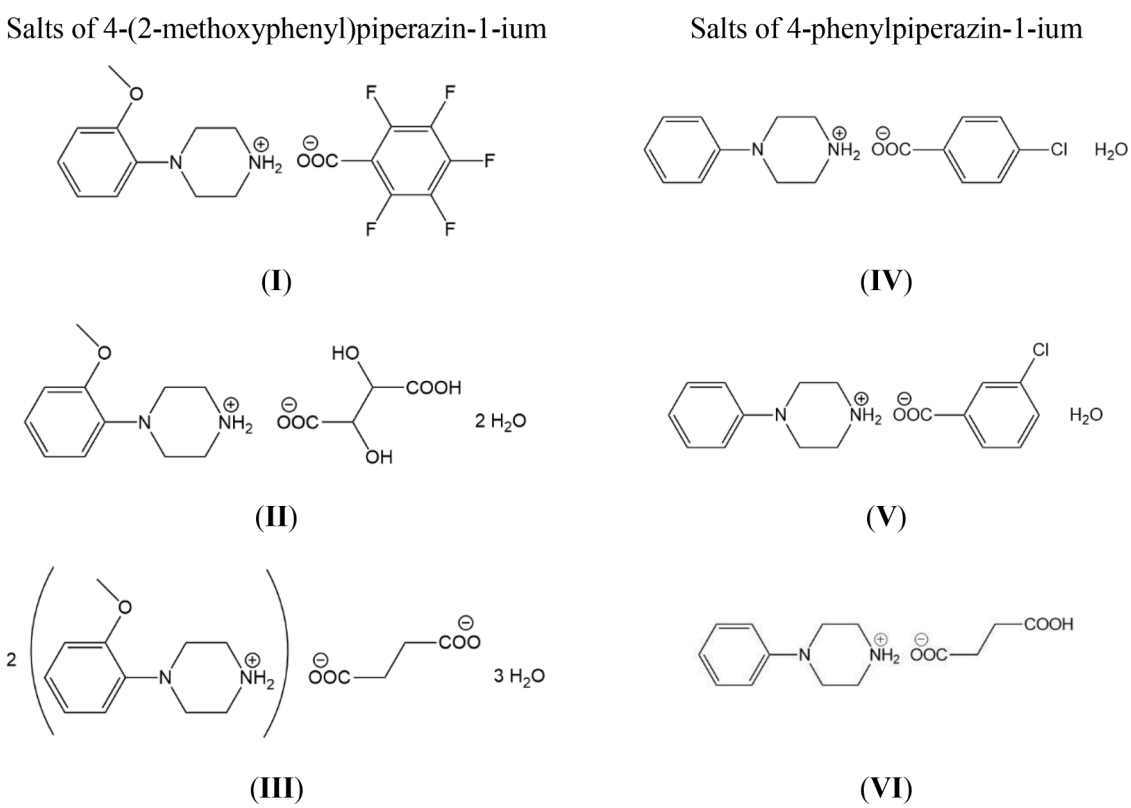

Scheme 1. Chemical structures of (I) – (VI).

carried out with *APEX3* [25]. The multi-scan absorption corrections were also applied [26]. The structures were solved by dual-space methods (*SHELXT* [27]) and refined by full-matrix least-squares procedures (*SHELXL2019* [28]). Additionally, extinction corrections were applied during refinement of structures (I) and (II).

The crystal of (VI) was found to be twinned by pseudo-merohedry with almost equal component occupancies (BASF=0.42172) transformed by a matrix of -1 0 0 / 0 -1 0 / 0 0 1, i.e., a two-fold rotation about its *c* axis [29]

The H atoms bonded to C atoms were included in the refinement using riding models, with constrained distances set to 0.95Å (aromatic), 0.98Å (R−CH_3), 0.99Å (R_2−CH_2) and 1.0Å (R_3−CH) (for R=C,N,O), and with $U_{iso}(H) = 1.2\ U_{eq}$ or $1.5\ U_{eq}$ (for R−CH_3 only) of the attached C atom.

The hydrogen atoms bonded to heteroatoms (N,O), involved in hydrogen bonds, were located in difference Fourier maps and refined freely.

In (II), water hydrogen atoms were refined with distance restraints (SADI in *SHELXL*).

In (III), the succinate anion was found to be disordered over two orientations with an occupancy ratio of 0.841(10):0.159(10). Moreover, a water molecule disordered across the inversion centre was modelled at half occupancy; U_{iso}(H) was constrained to 1.5 U_{eq}(O). To ensure satisfactory refinement for disordered groups in the structure, a combination of constraints and restraints was employed. Constraints (EXYZ and EADP) were used to fix overlapping fragments, whereas restraints (SAME, DFIX and FLAT) were used to maintain the structural integrity of disordered groups.

In (VI), a riding model was used for the donor groups of NH_2 [0.91Å, $U_{iso}(H)=1.2U_{eq}(N)$] and OH [0.84Å, $U_{iso}(H)=1.5U_{eq}(O)$].

The crystallographic data for compounds (I) – (VI) are summarized in Table 1.

2.4. Hirshfeld surface analysis

The *CrystalExplorer* program [23] was used to perform the Hirshfeld surface analysis [30]. For technical reasons, for compound (III), only the major component of disordered atoms in the succinate anion was taken into account, and a water molecule disordered around a centre of symmetry was excluded from calculations.

2.5. Pairwise model energies

The pairwise model energies, (CE-B3LYP) [24] between cation-anion pairs of the analysed salts (II), (IV) – (VI) were estimated using *CrystalExplorer* [23] using monomer wave functions at B3LYP/6-31G(d,p) levels along with Grimme's D2 dispersion corrections. Exclusion of (I) from the calculations was due to known technical problems; in case of (III), the reason is the lack of the balanced charge of the cation-dianion pair. The total interaction energy between ionic pairs was estimated in terms of four components: electrostatic, polarisation, dispersion, and exchange-repulsion, with scale factors of 1.057, 0.740, 0.871 and 0.618, respectively.

2.6. Single-point calculations

Single-point calculations were performed to estimate the binding energies for the cation-anion pairs of the investigated 4-(2-methoxyphenyl)piperazin-1-ium and 4-phenylpiperazin-1-ium salts (with the exception of compound (III), where the cation: anion ratio is 2:1 to ensure neutrality) and the corresponding salts published previously [11–13]). Calculations were carried out with the *Gaussian09* package [31] using a ωB97XD functional [32] with correction for long-range and dispersion effects and the basis set of 6-311++G(d,p) [33]. The selected ωB97XD functional offers more reliable results compared to other commonly used functionals [34]. For all pairs analysed that are connected by charge-assisted hydrogen bonds, the counterpoise correction was applied to estimate the basis set superposition error, BSSE [35]. The binding energies, which can be identified with intermolecular interaction energies, were calculated as the difference between the energy of the cation-anion pair and the sum of energies of monomers (cation and anion) that possess geometries taken from its pair.

Additionally, the binding energies of selected hydrogen-bonded ring systems of compounds (IV), $R_6^4(12)$ and $R_6^6(16)$, and (V), $R_6^5(14)$, were calculated at the same level of theory, however the BSSE correction was not applied so as to get comparable results with energies calculated previously for similar ring systems [36].

H-atom positions for all considered systems were taken directly from crystal structures and subsequently normalised according to mean X−H distances (X=C,N,O): d_{norm}(O−H)=0.993Å, d_{norm}(N−H)=1.015Å, d_{norm}(C−H)=1.089Å, implemented in *Mercury* software [37] to agree

Table 1
Experimental details for (I) – (VI).

	(I)	(II)	(III)	(IV)	(V)	(VI)
Crystal data						
Chemical formula	$C_7F_5O_2{\cdot}C_{11}H_{17}N_2O$	$C_{11}H_{17}N_2O{\cdot}C_4H_5O_6{\cdot}2(H_2O)$	$2(C_{11}H_{17}N_2O){\cdot}C_4H_4O_4{\cdot}3(H_2O)$	$C_{10}H_{15}N_2{\cdot}C_7H_4ClO_2{\cdot}H_2O$	$C_{10}H_{15}N_2{\cdot}C_7H_4ClO_2{\cdot}H_2O$	$C_{10}H_{15}N_2{\cdot}C_4H_5O_4$
M_r	404.33	378.38	556.65	336.81	336.81	280.32
Crystal system, space group	Monoclinic, $P2_1/n$	Monoclinic, $P2_1$	Triclinic, $P\overline{1}$	Monoclinic, $P2_1/c$	Monoclinic, $P2_1/c$	Monoclinic, Pn
a	14.2596 (6),	7.4715 (4),	7.3327 (3),	6.0483 (5),	18.6776 (6),	8.8024 (4),
b	5.5499 (3),	6.9855 (4),	9.8408 (6),	36.812 (3),	6.2169 (2),	26.9432 (11),
c (Å)	23.1124 (11)	17.7384 (10)	11.4595 (6)	7.4681 (7)	14.7105 (5)	11.8668 (5)
α, β, γ (°)	90, 98.518 (2), 90	90, 100.472 (1), 90	65.232 (2), 89.459 (2), 70.930 (2)	90, 95.155 (3), 90	90, 107.738 (1), 90	90, 90.012 (1), 90
V (Å^3)	1808.92 (15)	910.39 (9)	701.77 (6)	1656.1 (2)	1626.93 (9)	2814.4 (2)
Z	4	2	1	4	4	8
μ (mm^{-1})	0.14	0.98	0.10	0.25	0.25	0.81
Data collection						
No. of measured, independent, observed [$I > 2\sigma(I)$] reflections	27644, 4154, 3436	12953, 3515, 3498	23036, 3200, 2977	21224, 3840, 2874	29367, 3734, 3222	33795, 9773, 9725
R_{int}	0.036	0.027	0.035	0.058	0.041	0.034
$(\sin\theta/\lambda)_{max}$ (Å^{-1})	0.650	0.625	0.651	0.656	0.650	0.627
Refinement						
$R[F^2 > 2\sigma(F^2)]$, $wR(F^2)$, *S*	0.038, 0.079, 1.12	0.029, 0.074, 1.06	0.037, 0.096, 1.04	0.069, 0.139, 1.29	0.033, 0.085, 1.05	0.026, 0.068, 1.03
No. of reflections	4154	3515	3200	3840	3734	9773
No. of parameters/restraints	263/0	273/7	220/13	224/0	224/0	726/4
ρ_{max}, ρ_{min} (e Å^{-3})	0.22, -0.22	0.26, -0.20	0.38, -0.22	0.26, -0.44	0.33, -0.22	0.21, -0.15
Flack's parameter	–	-0.02 (4)	–	–	–	0.04 (4)

Experiments were carried out at 90 K with Mo *K*α (I, III, IV, V) or Cu *K*α radiation (II, VI) using a Bruker D8 Venture diffractometer.

with neutron diffraction data, as is recommended for most computational works [38].

3. Results

3.1. Structural characterization

The molecular structures of the asymmetric unit of compounds (I) – (VI) are visualised in Fig. 1 with the atom numbering scheme and anisotropic displacement parameters, using PLATON [39]. Compounds (I) and (VI) crystallize in solvent free forms, whereas (IV) and (V) are monohydrates. Redetermination of the salt (II) derived from (2*R*, 3*R*)-tartaric acid using Cu*K*α radiation shows that it is fully dihydrate; previously it has been reported with Mo*K*α as almost dihydrate (1.698 H_2O) [11]. In salt (III), the succinate dianion lies across a centre of inversion and is disordered, while the cation lies in a general position; the cation: anion ratio is 2:1, as required for charge balance; additionally, the structure was found to be a trihydrate. An unusual cation: anion ratio of 4: 4 is observed for compound (VI), which crystallises with the symmetry of the monoclinic *P*n space group.

The conformationally chiral cations, 2-MeOPP and PP, exist as racemic mixtures with the exception of compound (II), where only one

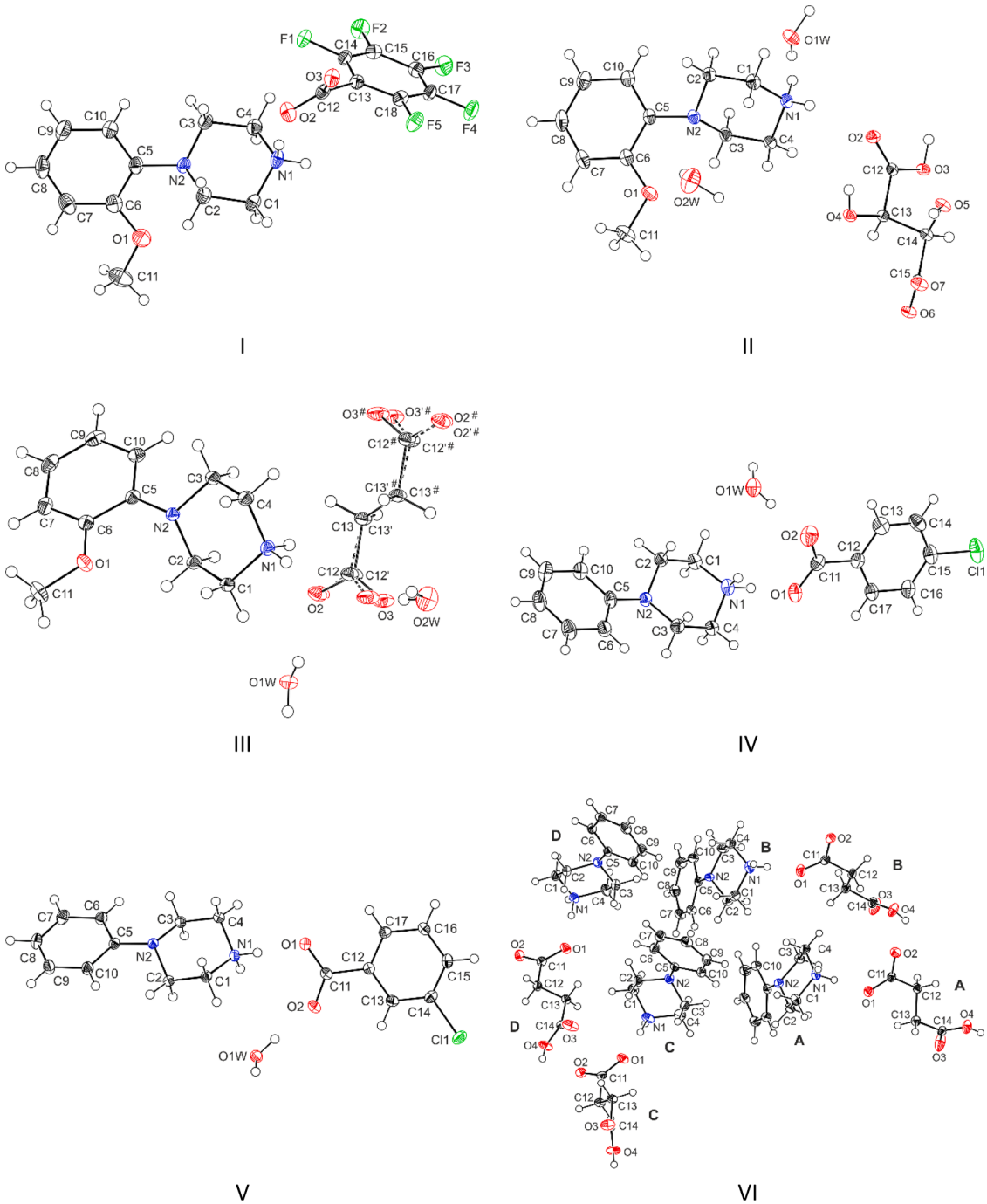

Fig. 1. Views of the asymmetric units of (I) – (VI) with the atom-numbering schemes. Displacement ellipsoids are drawn at the 50% probability level. In the asymmetric unit of (III), a half of the succinate dianion is independent; the major disorder component is drawn using full lines and the minor disorder component is drawn using broken lines. The atoms marked with a hash (#) are at the symmetry position (-*x*+1, -*y*+1, -*z*). The capital letters A – D indicate the independent moieties of (VI).

conformational enantiomer is present due to the Sohncke space group $P2_1$. In all compounds, the piperazine ring (N1/C1/C2/N2/C3/C4) adopts a chair conformation confirmed by the asymmetry parameters [40], ΔC_2 and ΔCs, ranging from 0.02(1)° to 8.2(2)°. The ring puckering parameters [41] differentiate the chair conformations from the asymmetric unit into two groups: with a θ value close to zero for cations in the asymmetric unit of (I), (II) and (VI, C and D molecules), as contrary to θ value close to 180° in the remaining cases. Both the methoxyphenyl and phenyl substituent occupy an equatorial site of the piperazine ring; the angle between the N1−C1 bond and the normal to the Cremer & Pople mean plane is close to 80°. In compounds (I) – (III) the methoxy group lies close to the best plane of the adjacent aryl ring; the maximum deviation of the C11 atom from that plane is -0.257(3)Å in (II).

In the anions, the negative charge of the carboxylate groups are weakly delocalized, which is indicated by the C−O bond lengths deviating by more than 3σ; the smallest and biggest differences are found for pentafluorobenzoate anion in (I), [1.2440(18)Å vs 1.2513(18)Å], and 4-chlorobenzoate anion in (IV) [1.242(4)Å vs 1.284(4)Å], respectively. Protons of the carboxylic group of tartrate (II) and succinate (VI) anions are correctly localized to the oxygen atom involved in the single C−O bond of ~1.3Å. The chiral tartrate anion exhibits *R,R* configurations of the asymmetric centres of C13 and C14 atoms.

3.2. Supramolecular assemblies in the salts

The supramolecular characterisation of the six arylpiperazine salts (I) – (VI) is based on hydrogen bonds with D−H···A angles greater than 120° and proton···acceptor distances shorter by 0.20Å than the sum of the van der Waals radii of the interacting atoms. To consider only the most structurally significant interactions in (III) the minor components of the disordered atoms (O2', O3', C12', C13') in the anion, and the water molecule disordered at the inversion centre were excluded from the analysis. The geometrical parameters describing hydrogen bonds are summarized in Table 2. Please note, that the notation of hydrogen bonds used in structural analysis does not contain information about donor and acceptor charges.

In (I), the cation and anion from the asymmetric unit are linked by a N1—H1*NB*···O2 hydrogen bond. An ion pair is further propagated along the *b* axis *via* N1—H1*NA*···O3(*x, y*-1, *z*) interaction forming a mono-periodic $C_2^2(6)$ chain motif [42–44] (Fig. 2*a*). Furthermore, the C4—H4*B*···F1 interaction supports an ionic pair, whereas C1—H4*C*···O3 (-*x*+1, -*y*+2, -*z*+1) links the adjacent chain pair to a column-like assembly whose centres coincide with the *b*-edges of the unit cell and its centre (Fig. 2*b*). There are no direction-specific interactions between molecular columns.

In (II), two hydroxyl groups and the carboxyl group of the tartrate anion act as donors in three O−H···O hydrogen bonds (Table 2) between adjacent anions, leading to formation of di-periodic (001) complex sheets. Water molecules and 2-MeOPP cations are attached to this sheet with the aryl groups sticking out (Fig. 3*b*). Within these sheets the O−H···O, N−H···O and O−H···N hydrogen bonds form a variety of ring motifs; some of them are presented in Fig. 3*a*: $R_1^2(5)$, $R_2^2(6)$, $R_2^2(11)$, $R_3^3(11)$, $R_4^3(11)$, $R_4^4(19)$; and some others as $R_4^3(8)$ and $R_6^5(19)$, etc. No other specific close contacts can be found between layers.

As shown in Fig. 4*a* the succinate anions and the water molecules in structure (III) are linked through O1*W*−H1*W*1···O2 and O1*W*−H2*W*1···O3(-*x*, -*y*+2, -*z*) hydrogen bonds to form a chain of centrosymmetric rings $R_4^4(12)$ running parallel to the [1$\bar{1}$0] direction. The cations combine these chains into di-periodic sheets lying parallel to (001). The arrangement of hanging 2-MeOPP moieties resembles a ladder-type formation (4*b*). The outermost aromatic aryl rings of the interpenetrating layers participate in two C−H···π(arene) contacts: C4−H4*B*···*Cg*(2-*x*, 1-*y*, 1-*z*) and C11−H11*A*···*Cg*(2-*x*, 2-*y*, 1-*z*) (*Cg* refers to the centre of gravity of the aryl ring).

The structures (IV) and (V) are isomeric; the anions are 4-chloroben-

Table 2
Hydrogen-bond geometry (Å,°) for (I) – (VI).

	D—H···*A*	*D*—H	H···*A*	*D*···*A*	∠ *D*—H···*A*
(I)	N1—H1*NA*···O3^{i}	0.904 (18)	1.896 (18)	2.7850 (17)	167.4 (15)
	N1—H1*NB*···O2	0.94 (2)	1.80 (2)	2.7300 (17)	171.6 (17)
	C1—H1*C*···O3^{ii}	0.99	2.45	3.392 (2)	159
	C4—H4*B*···F1	0.99	2.41	3.303 (2)	149
(II)	N1—H1*NA*···O3^{i}	0.84 (3)	2.32 (3)	2.943 (2)	131 (3)
	N1—H1*NA*···O6^{ii}	0.84 (3)	2.36 (3)	3.001 (2)	133 (3)
	N1—H1*NB*···O1*W*	0.94 (3)	1.88 (3)	2.805 (2)	168 (2)
	O3—H3···O7^{iii}	0.97 (4)	1.50 (4)	2.4689 (18)	174 (4)
	O4—H4···O6^{ii}	0.88 (3)	2.03 (3)	2.818 (2)	149 (2)
	O5—H5···O4^{ii}	0.77 (3)	2.09 (3)	2.766 (2)	147 (3)
	O1*W*—H1*W*1···O5^{iv}	0.98 (2)	1.75 (2)	2.721 (2)	173 (3)
	O1*W*—H2*W*1···O6^{i}	0.98 (2)	1.77 (2)	2.747 (2)	177 (4)
	O2*W*—H1*W*2···O1*W*^{v}	0.99 (2)	1.84 (2)	2.825 (2)	173 (4)
	O2*W*—H2*W*2···O1	0.99 (2)	2.16 (4)	3.041 (3)	147 (4)
	O2*W*—H2*W*2···N2	0.99 (2)	2.44 (4)	3.288 (3)	142 (4)
(III)	N1—H1*NA*···O2	0.959 (16)	1.747 (17)	2.702 (4)	173.4 (14)
	N1—H1*NA*···O2$'$	0.959 (16)	1.66 (3)	2.61 (2)	171.1 (17)
	N1—H1*NB*···O1*W*^{i}	0.917 (16)	1.813 (16)	2.7280 (12)	176.3 (14)
	O1*W*—H1*W*1···O2	0.85 (1)	1.96 (1)	2.733 (3)	150 (2)
	O1*W*—H1*W*1···O2$'$	0.85 (1)	1.96 (2)	2.701 (17)	146 (2)
	O1*W*—H2*W*1···O3^{ii}	0.85 (1)	1.86 (1)	2.6754 (16)	161 (2)
	O1*W*—H2*W*1···O3$'^{ii}$	0.85 (1)	1.94 (1)	2.714 (9)	152 (2)
(IV)	N1—H1*NB*···O1*W*^{i}	0.87 (4)	1.95 (4)	2.807 (3)	168 (3)
	N1—H1*NA*···O1	1.00 (4)	1.78 (4)	2.777 (3)	173 (3)
	C1—H1*D*···O1*W*	0.99	2.49	3.281 (4)	136
	C4—H4*B*···O1^{ii}	0.99	2.47	3.439 (4)	165
	O1*W*—H1*W*1···O2	0.81 (5)	1.84 (5)	2.638 (3)	168 (5)
	O1*W*—H2*W*1···O1^{iii}	0.88 (5)	1.90 (5)	2.770 (4)	169 (4)
(V)	N1—H1*NA*···O1	0.917 (19)	1.817 (19)	2.7280 (14)	171.7 (17)
	N1—H1*NB*···O1*W*^{i}	0.899 (17)	1.893 (18)	2.7604 (15)	161.4 (16)
	C1—H1*D*···O1*W*	0.99	2.42	3.305 (2)	149
	C4—H4*B*···O1^{ii}	0.99	2.46	3.432 (2)	166
	O1*W*—H1*W*1···O2	0.90 (2)	1.79 (2)	2.6789 (14)	172.5 (19)
	O1*W*—H2*W*1···O1^{iii}	0.88 (2)	1.85 (2)	2.7178 (14)	170.5 (19)
(VI)	N1*A*—H1*AA*···O1*A*	0.91	1.83	2.741 (3)	174
	N1*A*—H1*AB*···O2*B*^{i}	0.91	2.17	2.975 (3)	147
	O4*A*—H4*A*···O2*A*^{ii}	0.84	1.64	2.480 (3)	179
	C12*A*—H12*A*···O2*B*^{ii}	0.99	2.49	3.420 (3)	156
	N1*B*—H1*BA*···O2*A*^{iii}	0.91	1.99	2.853 (3)	159
	N1*B*—H1*BB*···O1*B*	0.91	1.83	2.735 (3)	174
	C1*B*—H1*BC*···O3*A*^{iv}	0.99	2.49	3.167 (3)	125
	O4*B*—H4*B*···O2*B*^{ii}	0.84	1.64	2.473 (3)	175
	N1*C*—H1*CA*···O2*D*^{v}	0.91	1.92	2.812 (3)	168
	N1*C*—H1*CB*···O1*C*	0.91	1.84	2.745 (3)	176
	C1*C*—H1*CC*···O4*C*^{vi}	0.99	2.46	3.250 (3)	137
	C1*C*—H1*CD*···O3*D*^{vii}	0.99	2.51	3.213 (4)	128
	C4*C*—H4*CA*···O3*D*^{vii}	0.99	2.47	3.186 (3)	129
	O4*C*—H4*C*···O2*C*^{viii}	0.84	1.62	2.461 (2)	177
	N1*D*—H1*DA*···O2*C*^{vi}	0.91	2.27	2.996 (3)	136
	N1*D*—H1*DA*···O3*C*^{ix}	0.91	2.30	2.879 (3)	122
	N1*D*—H1*DB*···O1*D*	0.91	1.81	2.719 (3)	173
	O4*D*—H4*D*···O2*D*^{viii}	0.84	1.65	2.489 (3)	173
	C12*D*—H12*F*···O2*C*^{x}	0.99	2.50	3.420 (3)	155

Symmetry codes: (I) (i) *x, y*-1, *z*; (ii) -*x*+1, -*y*+2, -*z*+1; (II) (i) -*x*+1, *y*-1/2, -*z*+1; (ii) -*x, y*-1/2, -*z*+1; (iii) *x*+1, *y, z*; (iv) -*x*+1, *y*+1/2, -*z*+1; (v) *x*-1, *y, z*; (III) (i) -*x*+1, -*y*+2, -*z*; (ii) -*x*, -*y*+2, -*z*; (IV) (i) -*x*+1, -*y*+1, -*z*+1; (ii) -*x*, -*y*+1, -*z*+2; (iii) *x*+1, *y, z*; (V) (i) -*x*+1, *y*+1/2, -*z*+3/2; (ii) -*x*+1, -*y*+2, -*z*+1; (iii) *x, y*-1, *z*; (VI) (i) *x*+1/2, -*y*+1, *z*-1/2; (ii) *x*-1/2, -*y*+1, *z*-1/2; (iii) *x*+1/2, -*y*+1, *z*+1/2; (iv) *x*+1, *y, z*+1; (v) *x*-1/2, -*y, z*-1/2; (vi) *x*-1/2, -*y, z*+1/2; (vii) *x*-1, *y, z*; (viii) *x*+1/2, -*y, z*-1/2; (ix) *x*-1, *y, z*+1; (x) *x*+1/2, -*y, z*+1/2.

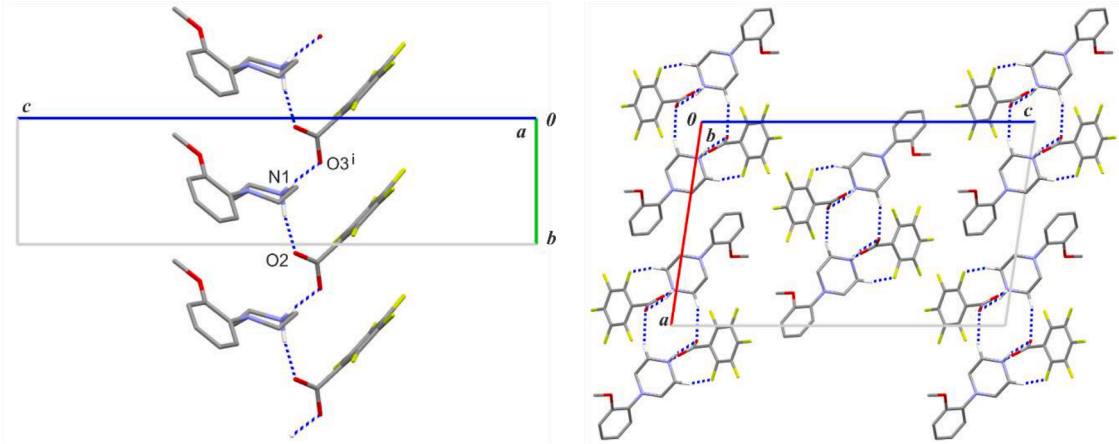

(*a*) (*b*)

Fig. 2. A chain motif in the crystal structure of (I) (*a*); a crystal packing diagram of (I) showing mono-periodic column-like assemblies in a view along the *b* axis (*b*). For the sake of clarity (for Figs. 1 – 8), C–H···O interactions have been omitted (*a*); (C)–H atoms not involved in hydrogen-bonds have been omitted (*a, b*). Symmetry code (i) *x, y*-1, *z*.

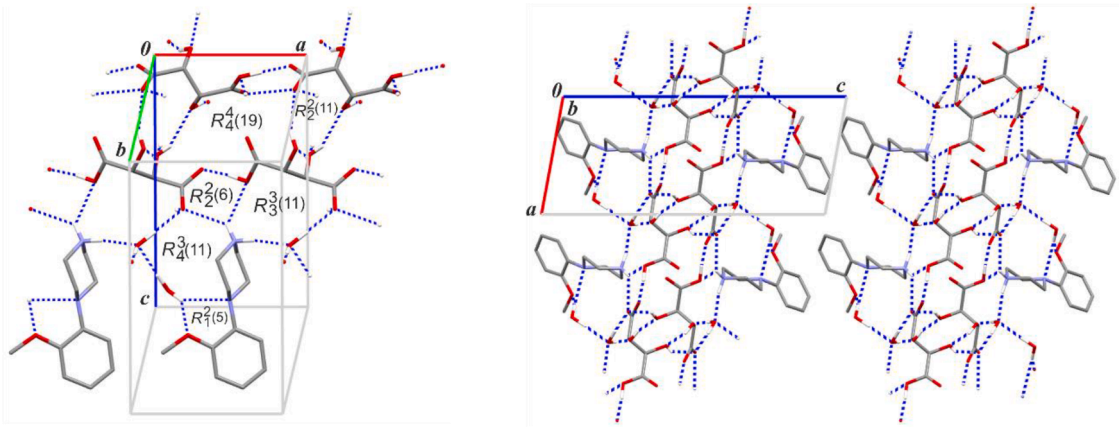

(*a*) (*b*)

Fig. 3. A part of the crystal structure of (II) showing the formation of miscellaneous hydrogen-bonded ring motifs (*a*); a crystal packing diagram of (II) showing di-periodic complex sheets in a view along the *b* axis (*b*).

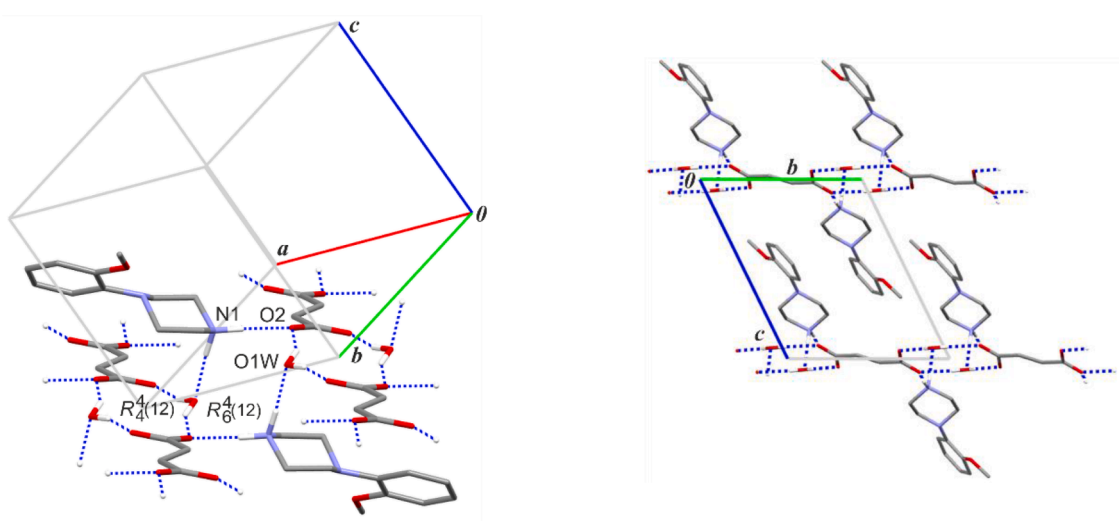

(*a*) (*b*)

Fig. 4. A part of the crystal structure of (III) showing the formation of di-periodic sheets (*a*); and their arrangements in a view along the *a* axis (*b*).

zoate in (IV) and 3-chlorobenzoate in (V), respectively; they are monohydrates. In both structures, the ionic components and the water molecules form a chain of edge-fused rings through the combination of N−H···O and O−H···O hydrogen bonds. Within a chain motif of (IV) running parallel to the [100] direction, two types of centrosymmetric rings can be distinguished: $R_6^4(12)$ and $R_6^6(16)$ (Fig. 5*a*), whereas in (V) the $R_6^5(14)$ rings are repeated around a 2_1-screw axis along *b* (Fig. 5*b*). Furthermore, in both structures, the C4−H4*B*···O1 interaction connects the chain-of-rings motifs along the [001] direction into di-periodic sheets. The C14−Cl1···Cl1(-*x*,1-*y*,1-*z*) halogen bond extends the supramolecular structure of (V) to a tri-periodic assembly (Fig. 7), in contrast to Cl···H contacts in (IV), which are not structurally significant and leave the di-periodic layers unchanged (Fig. 6). The chain-of-rings motif seems to be a quite typical hydrogen-bonding pattern for monohydrated arylpiperazin-1-ium salts with different benzoate anions mainly *p*-monosubstituted by halogens (F, Cl, Br), amino, hydroxyl, methoxy and ethoxy groups [36,45,46]. In our previous study [36] we estimated the binding energy of each ring motif [$R_6^4(12)$ and $R_6^6(16)$] constituting mono-periodic chains built from *N*-(4-methoxyphenyl)piperazin-1-ium cations, methoxy/ethoxy/ hydroxybenzoate anions and water molecules; they were found to be in the range from -1264.96 to -1275.15 kJ mol^{-1}, thus all of them have higher values than those estimated for ring motifs found in the investigated structures of (IV) and (V): -1229.32 for $R_6^4(12)$, -1220.89 for $R_6^6(16)$ and -1221.20 for $R_6^5(14)$, respectively (all energies are given in kJ mol^{-1}, BSSE uncorrected).

In (VI), both the ionic pairs A/B, and C/D are joined into di-periodic complex sheets in the (001) plane; the A/B assembly is generated relative to the glide plane every $\vec{b}$ lattice translation from the origin of the unit cell, whereas the C/D assembly is in the middle of the unit cell (Fig. 8). Within the hydrogen-bonded sheet, every PP cation interacts with two succinate anions, while every anion links to two cations and two anions. Similar to structures (II) and (III), anions segregate in the centre of the layer, whereas cations stick out to the outside.

3.3. Hirshfeld surface analysis

The similarities and differences in the analysed crystal structures can be visualised in part by Hirshfeld surface analysis. We modelled the Hirshfeld surface over the cations of (I) – (VI), and the corresponding fingerprint plots are depicted in Fig. S1 (Supplementary material). In all cases, the sharp spikes indicate that all cations donate (N)−H···O hydrogen bonds. In (II), a second, shorter spike can be found, which is derived from the reciprocal O/N···H−(O) contacts to the water molecule. Although structures (III) – (V) are also hydrated, the contacts with water are not as pronounced as for compound (II). Moreover, in the analysed salts, water molecules donate protons to anions rather than cations.

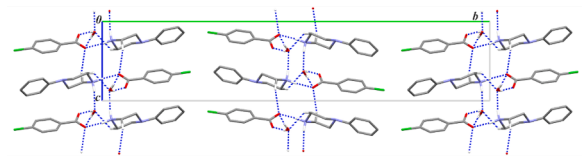

Fig. 6. A crystal packing of (IV) showing di-periodic sheets in a view along the *a* axis.

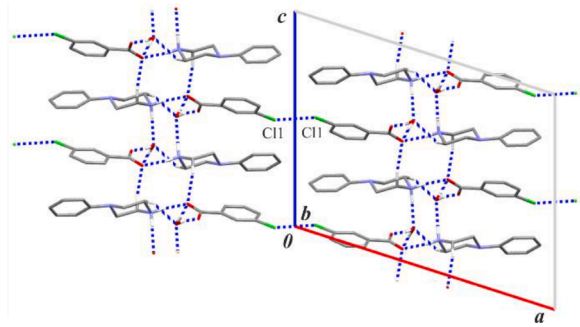

Fig. 7. A crystal packing of (V) showing the halogen bonds C14−Cl1···Cl1 in a view along the *b* axis.

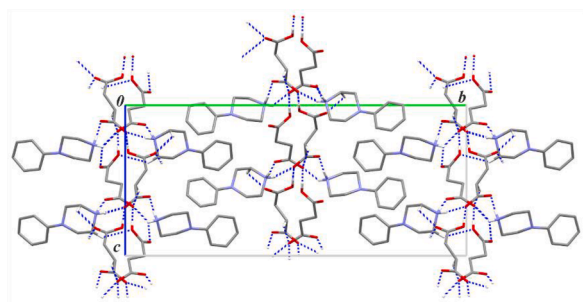

Fig. 8. A crystal packing of (VI) in a view along the *a* axis.

Fig. S3 presents the Hirshfeld fingerprint breakdown for the cations of compounds (I) – (VI). It can be seen that the environment of cation (I) differs most, having a relatively high contribution of H···F interactions to the Hirshfeld surface (26%) due to the presence of the pentafluorobenzoate anion. For cations (IV) and (V), the noticeable contributions of H···Cl contacts emerge accordingly to the chlorine substituent

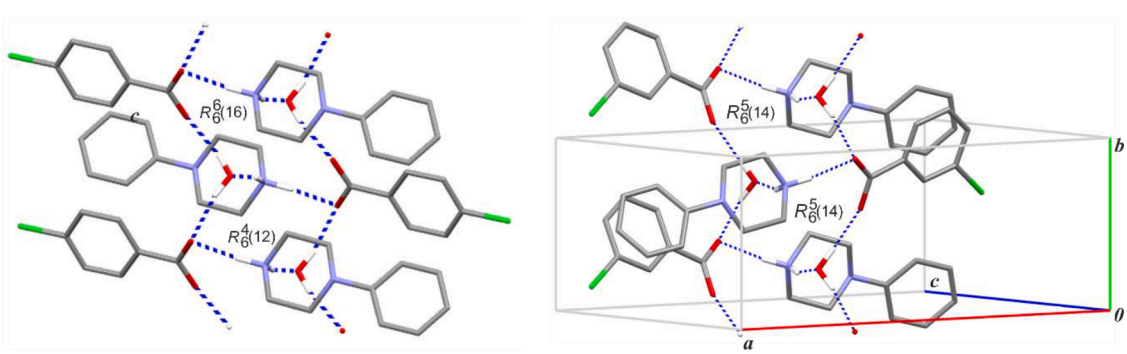

(*a*) (*b*)

Fig. 5. A part of the crystal structures of (IV) (*a*) and (V) (*b*) showing the formation of chain-of-rings motifs.

in the benzoate anion. It seems that the effects of the anion are mainly responsible for disturbances in the compatibility of the remaining contacts in the breakdown diagram. As is commonly observed, H···H contacts dominate with percentage contributions in the range of 58.3–62.7%, with exceptions of 36.9% for (I) and 48.3 % for (IV), respectively. About 20% of the surface corresponds to H···C contacts (except for IV, 26.3%). Statistically, the third biggest group of contacts are O···H interactions (13.1–20.4%). These are the most structurally important since they control the network architecture within each structure. The contribution of the remaining close interactions can be considered as negligible compared to groups mentioned above.

3.4. Binding energy of cation-anion pairs linked by charge-assisted hydrogen bonds

As pointed out in Section 3.3, all the analysed structures display a significant contribution of H···O contacts to the Hirshfeld surface of their cations. Examination of the arrangement of ionic species in the crystalline state of (I) – (VI) (Section 3.2) revealed that the positively charged N atom of the arylpiperazine moiety, 2-MeOPP and PP, due to proton transfer from the anion to the cation, prefers to form double charge-assisted hydrogen bonds, (+)N−H····O(-), with oxygen atoms of the carboxylate group of the accompanying anion. Moreover, the second (N)−H atom also can interact with another anion by symmetry or water molecule (for hydrated forms), and depending on the negatively charged/uncharged acceptor, CAHB(+/-) or CAHB(+) are formed. For the purpose of further analysis, we selected only cation-anion pairs that are formed by the cation of the asymmetric unit (ASU); the interactions with water molecules are excluded from the analysis because of the several times lower energies of such bridges in comparison to those of cation-anion pairs, even when the acceptor is an atom with a formally neutral charge. In the case of different stoichiometry other than 1:1, we accepted ionic pairs with a balanced charge of 0; thus for example for compound (VI), we analyse 9 pairs formed by A-D cations of the ASU. Others were excluded, for example, compound (II) with a doubly-ionized succinate moiety (stoichiometry cation: anion 2:1) was not considered. Finally, we have taken into account 72 ionic pairs from our present study and previously published salts of 2-MeOPP and PP cations [11–13]. Each pair has been characterized by normalised geometric parameters as H···O distance and N−H···O angle. For such ionic complexes, the binding energy, that can also be identified as intermolecular hydrogen-bond energy, has been estimated, as the energy required to separate monomers A and B to an infinite distance: $E_{binding}=E_{AB}-E_A-E_B$. The geometric and energetic parameters of all analysed pairs are listed in Tables S1 and S2 (Supplementary material).

Inspections of these tables indicate that the N atom of the piperazine moiety usually forms two hydrogen bonds with anions. The majority of considered anions are aromatic, only six are aliphatic. Twelve salts crystallize in hydrated forms, and compound (III), for which pairs were not considered. Charge-assisted hydrogen bonds in analysed anhydrous arylpiperazinium salts promote the formation of continuous chains or four-ion aggregates, whereas the chain of rings or di-periodic sheets are preferred for hydrated crystals.

In Fig. 9, we have plotted the binding energy for two sets of cations separately as a function of the normalised H···O distance. The two solid lines of trends have been drawn. The correlation coefficients are far from 1 but the sets of data are not typically homogenous and a quite large number of pairs is used for drawing such relationships. The lines intersect close to the distance of 2Å, which is thus quite clearly a cutoff point for the weakest interactions. Two points deviate substantially from the trends; it applies to ionic pairs of TEKWOY and TEKWIT (*Cambridge Structural Database* [47]; CSD refcodes) linked by (+)N−H···O hydrogen bonds. In Fig. 10, all pairs are used to draw the correlation. The plots demonstrate a known phenomenon that hydrogen-bond strengthening is accompanied by the shortening of the proton···acceptor distance. The weakest interactions are generally formed by pairs of cation-aliphatic

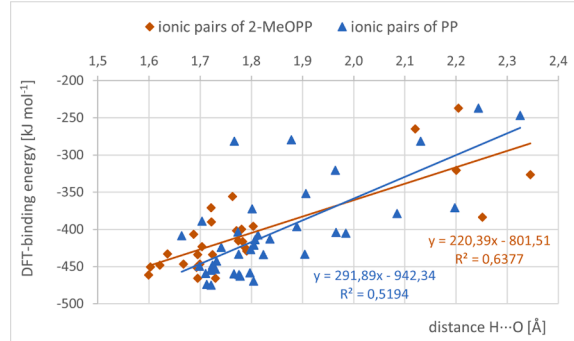

Fig. 9. Linear plots of counterpoise-corrected DFT-binding energies vs the normalised (N)H···O distance for ionic pairs; orange squares correspond to pairs of 2-MeOPP; blue triangles correspond to pairs of PP, respectively.

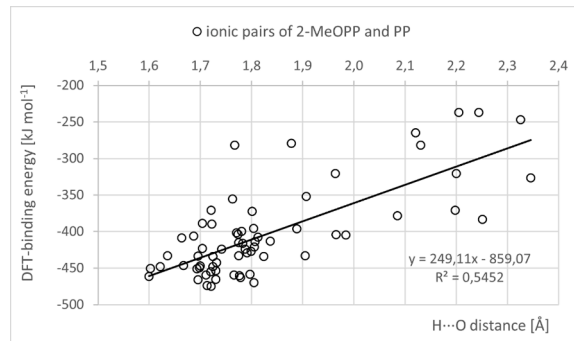

Fig. 10. Linear plot of counterpoise-corrected DFT-binding energies vs the normalised (N)H···O distance for all together ionic pairs of 2-MeOPP and PP (white circles).

anion of H···O distances longer than 2Å. The linear correlation between the normalized H···O distance vs N−H···O angle clearly confirms such a trend (Figs. 11 and 12); here the vast majority of pairs of cation-aliphatic anion demonstrates that its hydrogen-bonded bridges deviate far from linearity. This suggests, on average, that aromatic anions are engaged in stronger hydrogen bonding than the aliphatic ones. It seems to be associated with the expansion of the delocalization effect from the carboxylate group into the aromatic aryl ring, to which the group is directly attached.

For a set of 2-MeOPP and PP cations with small-organic anions, the overall range of estimated DFT-binding energies is from -237.02 to -474.84 kJ mol^{-1}, observed for pairs of compound (VI) and CSD:

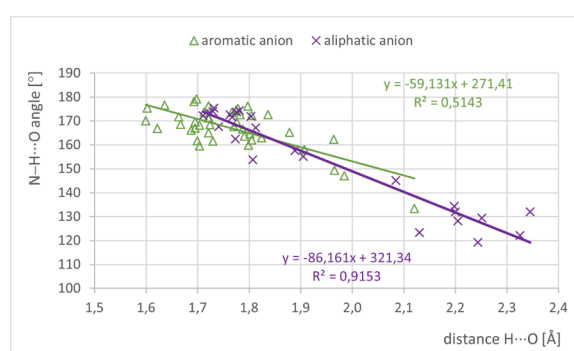

Fig. 11. The linear relationships between the normalised geometrical parameters: (N)H···O distance and the N−H···O angle, for ionic pairs of 2-MeOPP and PP cations: green open triangles correspond to aromatic anions; violet crosses correspond to aliphatic anions, respectively.

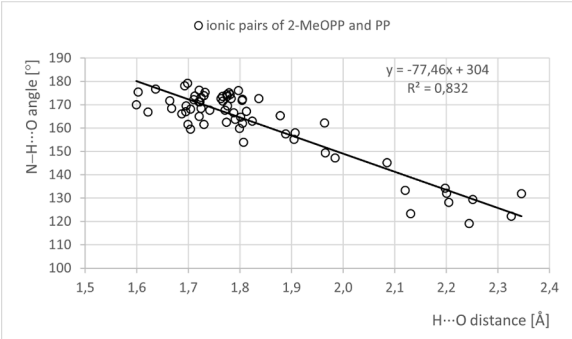

Fig. 12. The linear relationship between the normalised geometrical parameters: the (N)H···O distance and the N−H···O angle, for all together ionic pairs of 2-MeOPP and PP cations.

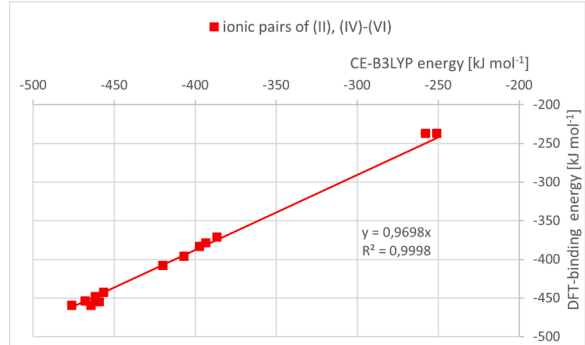

Fig. 13. The linear correlation of counterpoise-corrected DFT-binding energies vs CE-B3LYP model energies for ionic pairs of (II), (IV) – (VI).

YEDZEQ (PP with 4-methoxybenzoate monohydrate), respectively; an average value of all binding energies is -403.02 kJ mol^{-1}; the median value is -418.69 kJ mol^{-1}.

In Fig. 13 the DFT-binding energies (counterpoise-corrected) are compared with CE-B3LYP energies obtained by calculations in *CrystalExplorer* software, for cation-anion pairs of (II), (IV) – (VI). It is seen, that the energies agree very well (please note that the level of theory is different in the compared methods).

4. Conclusion

In this study, we have presented the structural characterisation of three salts each of the 4-(2-methoxyphenyl)piperazin-1-ium (2-MeOPP) and 4-phenylpiperazin-1-ium (PP) cations with simple organic-acid anions: pentafluorobenzoate, 4-chlorobenzoate, 3-chlorobenzoate, tartrate, and succinate. Structural investigations revealed that their supramolecular assemblies, from continuous chains to di-periodic sheets, are based on cation-anion pairs formed by charge-assisted hydrogen bonds (CAHBs), similarly to other recently published salts of 2-MeOPP and PP cations. To quantify the strength of the (+)N−H···O(-) and (+)N−H···O hydrogen bonds in 2-MeOPP and PP salts, we estimated DFT-binding energies of 72 ionic pairs. We have shown that the counterpoise-corrected energies of CAHBs are in the range from -237.02 to -474.84 kJ mol^{-1}. Both the linear plot for a relationship between the energy of the ionic pairs and the normalised H···O distance, as well as linear correlation between the H···O distance and the N−H···O angle, clearly show that the strongest interactions above 400 kJ mol^{-1} are characteristic for most pairs with aromatic anions with proton···acceptor distances shorter than 2Å and interaction angles greater than 150°. Consequently, the pairs of 2-MeOPP and PP cations with aliphatic anions demonstrate that their hydrogen-bonded bridges deviate far from linearity, resulting in lower binding energies. Furthermore, the pairwise energies (CE-B3LYP) calculated with *CrystalExplorer* for ionic pairs of (II), (IV) – (VI) confirm the electrostatic nature of the analysed CAHBs; their agreement with the DFT-energies suggests that both methods can be used for the energetic analysis of charge-assisted hydrogen bonds.

Credit author statement

H. J. Shankara Prasad, Devaraju, H. S. Yathirajan, C. N. Kavitha: Concept and design of the work; H. J. Shankara Prasad, H. G. A. Kumar, T. M. M. Kumar: Investigation; S. R. Parkin: Data collection, structure solution and refinement; L. Chęcińska: Theoretical calculations; L. Chęcińska, S. R. Parkin, H. S. Yathirajan: Interpretation of the results; L. Chęcińska, S. R. Parkin: Writing of article; L. Chęcińska, S. R. Parkin, H. S. Yathirajan: Correction of the final version

Declaration of Competing Interest

The authors declare that they have no known competing financial interests or personal relationships that could have appeared to influence the work reported in this paper.

Data availability

Data will be made available on request.

Acknowledgments

The D8 Venture diffractometer was funded by the NSF (MRI CHE1625732), and by the University of Kentucky. HJS is grateful to the DOS in Chemistry, University of Mysore for providing research facilities. HSY thanks UGC for a BSR Faculty fellowship for three years.

Supplementary materials

Supplementary material associated with this article can be found, in the online version, at doi:10.1016/j.molstruc.2023.136193.

References

[1] A.F. Brito, L.K.S. Moreira, R. Menegatti, E.A. Costa, Piperazine derivatives with central pharmacological activity used as therapeutic tools, Fundam. Clin. Pharmacol 33 (2019) 13–2413, https://doi.org/10.1111/fcp.12408.

[2] E. Bogatcheva, C. Hanrahan, B. Nikonenko, R. Samala, P. Chen, J. Gearhart, F. Barbosa, L. Einck, C.A. Nacy, M. Protopopova, Identification of new diamine scaffolds with activity against Mycobacterium tuberculosis, J. Med. Chem. 49 (2006) 3045–3048, https://doi.org/10.1021/jm050948+.

[3] L.L. Brockunier, J. He, L.F. Colwell, B. Habulihaz, H. He, B. Leiting, K.A. Lyons, F. Marsilio, R.A. Patel, Y. Teffera, J.K. Wu, N.A. Thornberry, A.E. Weber, E. R. Parmee, Substituted piperazines as novel dipeptidyl peptidase IV inhibitors, Bioorg. Med. Chem. Lett. 14 (2004) 4763–4766, https://doi.org/10.1016/j.bmcl.2004.06.065.

[4] M. Shaquiquzzaman, G. Verma, A. Marella, M. Akhter, W. Akhtar, M.F. Khan, S. Tasneem, M.M. Alam, Piperazine scaffold: a remarkable tool in generation of diverse pharmacological agents, Eur. J. Med. Chem. 102 (2015) 487–529, https://doi.org/10.1016/j.ejmech.2015.07.026.

[5] R.V. Patel, S.W. Park, An evolving role of piperazine moieties in drug design and discovery, Mini-Rev. Med. Chem. 13 (2013) 1579–1601, https://doi.org/10.2174/13895575113139990073.

[6] S. Demirci, T.B. Hayal, B. Kıratlı, H.B. Şişli, S. Demirci, F. Sahin, A. Doğan, Design and synthesis of phenylpiperazine derivatives as potent anticancer agents for prostate cancer, Chem. Biol. Drug Des. 94 (2019) 1584–1595, https://doi.org/10.1111/cbdd.13575.

[7] D.A. Horton, G.T. Bourne, M.L. Smythe, The combinatorial synthesis of bicyclic privileged structures or privileged substructures, Chem. Rev. 103 (2003) 893–930, https://doi.org/10.1021/cr020033s, 103.

[8] M. Perez, C. Fourrier, I. Sigogneau, P.J. Pauwels, C. Palmier, G.W. John, J. P. Valentin, S. Halazy, Synthesis and serotonergic activity of arylpiperazide derivatives of serotonin: potent agonists for 5-HT1D receptors, J. Med. Chem. 38 (1995) 3602–3607, https://doi.org/10.1021/jm00018a020.

[9] A. Hackling, R. Ghosh, S. Perachon, A. Mann, H.D. Höltje, C.G. Wermuth, J. C. Schwartz, W. Sippl, P. Sokoloff, H. Stark, N-(ω-(4-(2-Methoxyphenyl)piperazin-

1-yl)alkyl)carboxamides as dopamine D2 and D3 receptor ligands, J. Med. Chem. 46 (2003) 3883–3899, https://doi.org/10.1021/jm030836n.
[10] A.M. Waszkielewicz, K. Pytka, A. Rapacz, E. Wełna, M. Jarzyna, G. Satała, A. Bojarski, J. Sapa, P. Żmudzki, B. Filipek, H. Marona, Synthesis and evaluation of antidepressant-like activity of some 4-substituted 1-(2-methoxyphenyl)piperazine derivatives, Chem. Biol. Drug Des. 85 (2015) 326–335, https://doi.org/10.1111/cbdd.12394.
[11] C. Harish Chinthal, C.N. Kavitha, H.S. Yathirajan, S. Foro, R.S. Rathore, C. Glidewell, Fifteen 4-(2-methoxyphenyl)piperazin-1-ium salts containing organic anions: supramolecular assembly in zero, one, two and three dimensions, Acta Crystallogr. E76 (2020) 1779–1793, https://doi.org/10.1107/S2056989020014097.
[12] N. Mahesha, H.K. Kumar, M. Akkurt, H.S. Yathirajan, S. Foro, M.S.M. Abdelbaky, S. Garcia-Granda, Crystal-structure studies of 4-phenylpiperazin-1-ium 4-etoxybenzoate monohydrate, 4-phenylpiperazin-1-ium 4-methoxybenzoate monohydrate, 4-phenylpiperazin-1-ium 4-methylbenzoate monohydrate and 4-phenylpiperazin-1-ium trifluoroacetate 0.12-hydrate, Acta Crystallogr. E78 (2022) 709–715, https://doi.org/10.1107/S2056989022006004.
[13] S.D. Archana, H. Kiran Kumar, H.S. Yathirajan, S. Foro, R.J. Butcher, The structures of eleven (4-phenyl)piperazinium salts containing organic anions, Acta Crystallogr. E78 (2022) 1016–1027, https://doi.org/10.1107/S2056989022009057.
[14] G.A. Jeffrey, An Introduction to Hydrogen Bonding, Oxford University Press, New York, NY, USA, 1997.
[15] D. Braga, L. Maini, F. Lucia, A Grepioni, O. De Cian, J. Félix, M.W. Fischer, Charge-assisted N–H(+)···O(−) and O–H···O(−) hydrogen bonds control the supramolecular aggregation of ferrocenedicarboxylic acid and bis-amidines, New J. Chem. 24 (2000) 547–553, https://doi.org/10.1039/B002061N.
[16] Y. Zhang, Y. Li, Y. Zhang, L. Liu, D. Zou, W. Sun, J. Li, Y. Feng, Y. Geng, G. Cheng, Improved solubility and hygroscopicity of enoxacin by pharmaceutical salts formation with hydroxybenzonic acids via charge assisted hydrogen bond, J. Mol. Struct. 1273 (2023), 134272, https://doi.org/10.1016/j.molstruc.2022.134272.
[17] K. Kazimierczuk, Charge-assisted $N^{(+)}$–H···$^{(-)}$S hydrogen bonds in the crystal structure of selected diammonium thiophenolates, Struct. Chem. 27 (2016) 1005–1016, https://doi.org/10.1007/s11224-015-0733-2.
[18] S.A. Katsyuba, M.V. Vener, E.E. Zvereva, Z. Fei, R. Scopelliti, J.G. Brandenburg, S. Siankevich, P.J. Dyson, Quantification of conventional and nonconventional charge-assisted hydrogen bonds in the condensed and gas phases, J. Phys. Chem. Lett. 6 (2015) 4431–4436, https://doi.org/10.1021/acs.jpclett.5b02175.
[19] B. Bankiewicz, P. Matczak, M. Palusiak, Electron density characteristics in bond critical point (QTAIM) versus interaction energy components (SAPT): The case of charge-assisted hydrogen bonding, J. Phys. Chem. A116 (2012) 452–459, https://doi.org/10.1021/jp210940b.
[20] S.J. Grabowski, Theoretical studies of strong hydrogen bonds, Annu. Rep. Prog. Chem. Sect. C Phys. Chem 102 (2006) 131–165, https://doi.org/10.1039/B417200K.
[21] Vol. Ed M.D. Ward, M.W. Hosseini, Charge-assisted hydrogen-bonded networks, in: Molecular Networks, 132, Springer-Verlag, Berlin Heidelberg, 2009, pp. 1–23. Vol. EdStruct. Bond2009.
[22] M.D. Ward, Design of crystalline molecular networks with charge-assisted hydrogen bonds, Chem. Commun. (2005) 5838–5842, https://doi.org/10.1039/B513077H.
[23] M.J. Turner, J.J. McKinnon, S.K. Wolff, D.J. Grimwood, P.R. Spackman, D. Jayatilaka, M.A. Spackman, *CrystalExplorer17.5*. University of Western Australia, 2017.
[24] M.J. Turner, S. Grabowsky, D. Jayatilaka, M.A. Spackman, Accurate and efficient model energies for exploring intermolecular interactions in molecular crystals, J. Phys. Chem. Lett. 5 (2014) 4249–4255, https://doi.org/10.1021/jz502271c.
[25] Bruker-AXS. APEX3; Bruker-AXS Inc.: Madison, WI, USA, 2016.
[26] L. Krause, R. Herbst-Irmer, G.M. Sheldrick, D. Stalke, Comparison of silver and molybdenum microfocus X-ray sources for single-crystal structure determination, J. Appl. Cryst. 48 (2015) 3–10, https://doi.org/10.1107/S1600576714022985.
[27] G.M. Sheldrick, SHELXT-integrated space-group and crystal-structure determination, Acta Crystallogr. A71 (2015) 3–8, https://doi.org/10.1107/S2053273314026370.
[28] G.M. Sheldrick, Crystal structure refinement with SHELX, Acta Crystallogr. (2015) 3–8, https://doi.org/10.1107/S2053229614024218. C71.
[29] S.R. Parkin, Practical hints and tips for solution of pseudo-merohedric twins: three case studies, Acta Crystallogr. E77 (2021) 452–465, https://doi.org/10.1107/S205698902100342X.
[30] M.A. Spackman, D. Jayatilaka, Hirshfeld surface analysis, CrystEngComm 11 (2009) 19–32, https://doi.org/10.1039/B818330A.
[31] M.J. Frisch, G.W. Trucks, H.B. Schlegel, G.E. Scuseria, M.A. Robb, J.R. Cheeseman, G. Scalmani, V. Barone, B. Mennucci, G.A. Petersson, et al., Gaussian 09, Gaussian Inc., Wallingford, CT, USA, 2013. Rev. D.01.
[32] J.D. Chai, M. Head-Gordon, M. Long-range corrected hybrid density functionals with damped atom–atom dispersion corrections, Phys. Chem. Chem. Phys. 10 (2008) 6615–6620, https://doi.org/10.1039/B810189B.
[33] R. Krishnan, J.S. Binkley, R. Seeger, J.A. Pople, Self-consistent molecular-orbital methods. XX. A basis set for correlated wave-functions, J. Chem. Phys. 72 (1980) 650–654, https://doi.org/10.1063/1.438955.
[34] Y. Minenkov, Å. Singstad, G. Occhipinti, V.R. Jensen, The accuracy of DFT-optimized geometries of functional transition metal compounds: a validation study of catalysts for olefin metathesis and other reactions in the homogeneous phase, Dalton Trans. 41 (2012) 5526–5541, https://doi.org/10.1039/C2DT12232D.
[35] S.F. Boys, F. Bernardi, The calculation of small molecular interactions by the differences of separate total energies. Some procedures with reduced errors, Mol. Phys. 19 (1970) 553–561, https://doi.org/10.1080/00268977000101561.
[36] P. Priyanka, B.K. Jayanna, T.R Divakara, G.P. Suresha, Vinaya, Y.B Basavaraju, H. S Yathirajan, S.R. Parkin, L. Chęcińska, Hydrogen-Bonded Chain of Rings Motif in N-(4-Methoxyphenyl)piperazin-1-ium Salts with Benzoate Anions: Supramolecular Assemblies and Their Energy Frameworks, Crystals 12 (2022), 1807, https://doi.org/10.3390/cryst12121807.
[37] C.F. Macrae, I. Sovago, S.J. Cottrell, P.T.A. Galek, P. McCabe, E. Pidcock, M. Platings, G.P. Shields, J.S. Stevens, M. Towler, P.A. Wood, Mercury 4.0: From visualization to analysis, design and prediction, J. Appl. Cryst. 53 (2020) 226–235, https://doi.org/10.1107/S1600576719014092.
[38] F.H. Allen, I.J. Bruno, Bond lengths in organic and metal-organic compounds revisited: X—H bond lengths from neutron diffraction data, Acta Crystallogr. B66 (2010) 380–386, https://doi.org/10.1107/S0108768110012048.
[39] A.L. Spek, checkCIF validation ALERTS: what they mean and how to respond, Acta Crystallogr. E76 (2020) 1–11, https://doi.org/10.1107/S2056989019016244.
[40] L. Duax, D.A. Norton, Atlas of Steroid Structure; IFI/Plenum: New York, NY, USA. 1975, 1, 16–22.
[41] D. Cremer, J.A. Pople, General definition of ring puckering coordinates, J. Am. Chem. Soc. 97 (1975) 1354–1358, https://doi.org/10.1021/ja00839a011.
[42] J. Bernstein, R.E. Davis, L. Shimoni, N.L. Chang, Patterns in hydrogen bonding: functionality and graph set analysis in crystals, Angew. Chem. Int. Ed. Engl. 34 (1995) 1555–1573, https://doi.org/10.1002/anie.199515551.
[43] M.C. Etter, Encoding and decoding hydrogen-bond patterns of organic compounds, Acc. Chem. Res. 23 (1990) 120–126, https://doi.org/10.1021/ar00172a005.
[44] M.C. Etter, J.C. MacDonald, J. Bernstein, Graph-set analysis of hydrogen-bond patterns in organic crystals, Acta Crystallogr. B46 (1990) 256–262, https://doi.org/10.1107/S0108768189012929.
[45] H. Kiran Kumar, H.S. Yathirajan, S. Foro, C. Glidewell, Crystal structures of the recreational drug N-(4-methoxyphenyl)piperazine (MeOPP) and three of its salts, Acta Crystallogr. E76 (2020) 488–495, https://doi.org/10.1107/S2056989020002844.
[46] H. Kiran Kumar, H.S. Yathirajan, S. Foro, C. Glidewell, Twelve 4-(4-methoxyphenyl)piperazin-1-ium salts containing organic anions: supra-molecular assembly in one, two and three dimensions, Acta Crystallogr. E75 (2019) 1494–1506, https://doi.org/10.1107/S2056989019012702.
[47] C.R. Groom, J.J. Bruno, M.P. Lightfoot, S.C. Ward, The Cambridge structural database, Acta Crystallogr. B72 (2016) 171–179, https://doi.org/10.1107/S2052520616003954.